L-cysteine-capped core/shell/shell quantum dot-graphene oxide nanocomposite fluorescence probe for polycyclic aromatic hydrocarbon detection

Oluwasesan Adegoke, Patricia B.C. Forbes*

Department of Chemistry, Faculty of Natural and Agricultural Sciences, University of Pretoria, Lynnwood Road, Pretoria 0002, South Africa

*Corresponding author:

Email address: adegoke.sesan@mailbox.co.za (O. Adegoke), patricia.forbes@up.ac.za (P.B.C. Forbes)

Highlights

- CdSeTe/ZnSe/ZnS quantum dots were synthesized for the first time.
- A novel soluble quantum dot–graphene oxide (QD–GO) nanocomposite was prepared.
- Four ubiquitous PAHs were tested for their affinity to the novel QD–GO probe.
- The LOD for phenanthrene in water was 0.19 µg/L.
- Detection may be based on an adsorption-fluorescence enhancement effect.

Graphical abstract

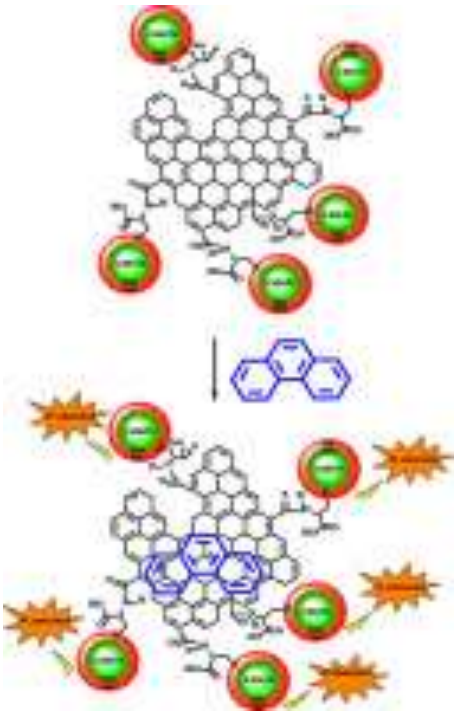

Abstract

Environmental pollutants, such as the polycyclic aromatic hydrocarbons (PAHs), become widely distributed in the environment after emission from a range of sources, and they have potential biological effects, including toxicity and carcinogenity. In this work, we have demonstrated the analytical potential of a covalently linked L-cysteine-capped CdSeTe/ZnSe/ZnS core/shell/shell quantum dot (QD)-graphene oxide (GO) nanocomposite fluorescence probe to detect PAH compounds in aqueous solution. Water-soluble L-cysteine-capped CdSeTe/ZnSe/ZnS QDs were synthesized for the first time and were covalently bonded to GO. The fluorescence of the QD-GO nanocomposite was enhanced relative to the unconjugated QDs. Various techniques including TEM, SEM, HRSEM, XRD, Raman, FT-IR, UV/vis and fluorescence spectrophotometry were employed to characterize both the QDs and the QD-GO nanocomposite. Four commonly found priority PAH analytes namely; phenanthrene (Phe), anthracene (Ant), pyrene (Py) and naphthalene (Naph), were tested and it was found that each of the PAH analytes enhanced the fluorescence of the QD-GO probe. Phe was selected for further studies as the PL enhancement was significantly greater for this PAH. A limit of detection (LOD) of 0.19 μg/L was obtained for Phe under optimum conditions, whilst the LOD of Ant, Py and Naph were estimated to be ~0.26 μg/L. The fluorescence detection mechanism is proposed.

Keywords: Quantum dots; Graphene oxide; Adsorption; Photoluminescence; Polycyclic aromatic hydrocarbon; Fluorescence sensor

1. Introduction

Potentially harmful pollutants such as polycyclic aromatic hydrocarbons (PAHs) are emitted into the environment as a consequence of combustion processes such as cigarette burning, petrol and diesel engine operation, coal combustion and waste incineration **[1,2].** Hence, the presence of PAHs in the environment is of health concern **[3]** and requires extensive monitoring.

High performance liquid chromatography (HPLC) and gas chromatography (GC) are typically employed for the environmental monitoring of PAHs **[4,5].** Although these methods have proven successful, they often require analyte extraction and cleanup prior to analysis. In addition, the instrumentation required is expensive, which may limit the extent of monitoring possible in developing countries, where resources are limited **[6]**. The development of rapid, simple, sensitive and selective methods for screening environmental samples for PAHs is therefore an attractive alternative. Recently, carbon-based materials such as graphene and graphene oxide (GO), which exhibit a single sp^2 layered hybridized carbon atom bonded in a covalent honeycomb-like crystal lattice has emerged as a useful adsorbent material for the preconcentration of several environmental organic pollutants containing fused benzene rings from both air and water matrices **[7-10]**. The superior adsorptive power of graphene-based materials is due to their large delocalized π electrons and high surface area **[11]**. Organic pollutants containing fused rings can adsorb onto graphene via various mechanisms such as electrostatic interaction, non-covalent interaction, hydrogen bonding, dispersion forces, hydrophobic interactions, dative bonds and Van der Waals interactions **[12]**. However, despite these advantages

exhibited by graphene-based materials, they tend to restack to graphite and are prone to aggregation when applied in bulk quantities during adsorption processes **[13]**. Additionally, the strong interplanar interactions within their system also limit their use **[13]**. These disadvantages can be overcome via covalent or non-covalent interactions of graphene-based materials with other nanomaterials or molecules of interest **[14]**. An enhancement in selectivity, sensitivity and limit of detection (LOD) of graphene-based materials can be achieved by bonding with other nanoparticles **[15,16].**

After two decades of intense pioneering research on the surface chemistry and optical properties of QDs nanocrystals, colloidal semiconductor QD nanoparticles have now garnered considerable research attention due to their unique properties including bright fluorescence, narrow emission and broad absorption spectra, size-tunable fluorescence spectra, excellent photostability and multiplex colour potentials. They therefore have promising applications such as in biolabeling, bioimaging, biotracking of drug molecules, sensing/biosensing, photodynamic therapy, molecular biology and antimicrobial prevention, etc **[17,18].**

Bonding of QDs to graphene-based materials to form nanocomposite probes for the detection of analytes such as hydrogen peroxide **[19],** chloramphenicol **[20]**, lead ions **[21]** and glucose **[22]** have been reported**.** To the best of our knowledge, there are no reports on the use of QD-GO for the fluorescent detection of PAHs. In this work, we have successfully synthesized CdSeTe/ZnSe/ZnS QD core/shell/shell nanoparticles for the first time via a facile one-pot approach and then converted the hydrophobic QDs to the hydrophilic phase via a ligand exchange reaction with L-cysteine thiol

ligand. The choice of the alloyed QD core and the passivation with a Zn-based double shell is to ensure the Cd ion is strongly protected against leakage, hence ensuring the QDs do not pose any form of toxicity or environmental impact in use. The newly synthesized QDs were covalently bonded to GO to form a novel QD-GO nanocomposite probe, which we investigated for use as a fluorescent probe to detect commonly found PAHs in water. The simplicity of the newly developed QD-GO nanocomposite sensor takes advantage of the adsorptive power and delocalized π interactions of graphene, which enhance adsorption of PAH compounds with consequent enhancement of the QD fluorescence.

2. Experimental

2.1. Materials

Trioctylphosphine oxide (TOPO), N-(3-Dimethylaminopropyl)-N′-ethylcarbodiimide hydrochloride (EDC), N-Hydroxysuccinimide (NHS), cadmium oxide, octadec-1-ene (ODE), tellurium powder (Te), zinc oxide, zinc diethyldithiocarbamate (ZDC), L-cysteine, oleic acid (OA) and PAH standards consisting of pyrene (Py), anthracene (Ant), naphthalene (Naph) and phenanthrene (Phe) were purchased from Sigma Aldrich. Hydrogen peroxide, sulphuric acid (H_2SO_4), methanol, absolute ethanol, sodium nitrate ($NaNO_3$), chloroform, acetone, hydrochloric acid (HCl), selenium powder (Se), graphite powder, potassium hydroxide (KOH) and potassium permanganate ($KMnO_4$) were purchased from Merck. An ultrapure Milli-Q Water System was used for sample preparation.

2.2. Apparatus

UV-vis absorption spectra were recorded on a Cary Eclipse (Varian) spectrophotometer. Fluorescence emission spectra were recorded on a Horiba Jobin Yvon Fluoromax-4 spectrofluorometer. Determination of the PL quantum yield (Φ_F) of the QDs was achieved by comparing the integrated fluorescence intensities of the QDs (*F*) in Millipore water to that of Rhodamine 6G (F_{Std} ; $\Phi_{F(Std)}$ = 95% **[23]**) in ethanol whilst taking into consideration the refractive indices (*n*) of the solvents and absorbance of each QDs (*A*) and Rhodamine 6G (A_{Std}) at the excitation wavelength.

$$\Phi_F = \Phi_{F(Std)} \frac{F \,.\, A_{Std} \,.\, n^2}{F_{Std} \,.\, A \,.\, n_{Std}^2}$$

Powder X-ray diffraction (XRD) patterns were analyzed using a PANalytical X'Pert Pro powder diffractometer in θ–θ configuration with an X'Celerator detector, variable divergence and receiving slits with Fe filtered Co-Kα radiation (λ=1.789Å). Transmission electron microscopy (TEM) images were obtained using a JEOL JEM 2100F operated at 200 kV. Raman analyses were performed using a T64000 micro-Raman spectrometer (HORIBA Scientific Jobin Yvon Technology) equipped with a triple monochromator system to eliminate contributions from the Rayleigh line. Scanning electron microscopy (SEM) measurements were carried out using a JEOL JSM-5800LV operated at 20kV. High resolution scanning electron microscopy (HRSEM) measurements were carried out using an FE-SEM Zeiss Ultra Plus. FT-IR analyses were performed using a Bruker Vertex 70V.

2.3. Synthesis of CdSeTe/ZnSe/ZnS core/shell/shell QDs

The one-pot synthesis of CdSeTe/ZnSe/ZnS QDs was carried out based on a reported procedure for the synthesis of core/shell/shell QDs **[24],** with modifications**.** Briefly, 1.3 g of CdO was added into a solution of 50 mL of QDE and 30 mL of OA and the solution was vigorously stirred in a 3-necked flask under argon atmosphere to a temperature of 260 ^{o}C in order to form a colourless Cd-OA complex. Once the colourless complex solution was formed, a premixed TOPTe solution containing 0.48 g of Te and 1.93 g of TOPO in 25 mL of ODE was added into the solution and this was followed swiftly by the addition of a TOPSe solution containing 0.30 g of Se and 1.93 g of TOPO in 25 mL of ODE. Nucleation and growth of the alloyed core QDs was allowed to proceed for ~15 min after which a ZnO solution containing 0.41 g of ZnO dissolved in 20 mL of OA and 30 mL of ODE was injected into the growth solution and this was followed immediately by the addition of the TOPSe solution. This resulted in the overcoating of the ZnSe shell around the alloyed CdSeTe core surface. Passivation of the CdSeTe/ZnSe core/shell QDs with a ZnS shell was carried out by adding into the core/shell growth solution, 0.407 g of ZDC dissolved in 30 mL of ODE and 20 mL of OA. ZDC was employed as a single molecular precursor because it dissolves in solution to form ZnS metal sulfide **[25]**. The CdSeTe/ZnSe/ZnS QDs were allowed to react for around 2 hrs. Purification of the hydrophobic QDs was carried out using methanol followed by acetone.

2.4. Water solubilization of the CdSeTe/ZnSe/ZnS QDs

Water solubilization of the QDs was carried out via a ligand exchange reaction with L-cysteine thiol ligand as a hydrophilic capping agent. Firstly, a KOH-methanolic-L-cysteine solution was prepared by dissolving 3.0 g of KOH in 40 mL of methanol and 2.0 g of L-cysteine was then dissolved in the solution via ultrasonication. Afterward, the hydrophobic CdSeTe/ZnSe/ZnS QDs were dispersed in chloroform and added into the KOH-methanolic-L-cysteine solution followed by the addition of Millipore water. This resulted in the separation of the organic phase from the water-soluble phase. The solution was stirred for 15 min and was then purified as follows: step 1: acetone; step 2: chloroform; step 3: water:chloroform:acetone (1:1:2) mixture; and step 4: chloroform followed by acetone. The rigorous purification steps were carried out to remove the high level of unreacted organic layers embedded on the surface of the QDs.

2.5. Synthesis of GO nanosheets

GO nanosheets were prepared based on the modified Hummers method **[26].** Graphite oxide was firstly synthesized and then chemically exfoliated to form GO. Briefly, in a 250 mL round bottom flask, 60 mL of H_2SO_4 was added and cooled with ice. Then 2.5 g of graphite powder and 1.25 g of $NaNO_3$ were added and the solution was vigorously stirred to allow for thorough dispersion of the graphite powder. Afterward, 7.5 g of $KMnO_4$ was added and the solution was kept in ice for few hours and thereafter the ice bath was removed and the reaction mixture was stirred under ambient temperature overnight which resulted in the formation of a pasty light

brown coloured mixture. The reaction mixture was then placed in an ice bath and 75 mL of Millipore water was slowly added under stirring. The temperature of the solution was raised to 60 ^{o}C and allowed to stir overnight. The following day, 25 mL of 30% H_2O_2 was added to the reaction mixture, which was then centrifuged with 5% HCl solution followed by Millipore water in order to remove unreacted metal ions. The prepared graphite oxide (yield = 4.0 g) was dried at 65 ^{o}C and a grey powder was obtained.

To form the GO nanosheets, 0.8 g of graphite oxide was dispersed in Millipore water and was then exfoliated via ultrasonication for ~3 hrs. Finally, the solution was purified with 5% HCl solution and dried at 65 ^{o}C. The yield of the purified GO nanosheets was 0.4 g.

2.6. Preparation of QD-GO nanocomposite

Scheme 1 depicts the process employed in the preparation of the QD-GO nanocomposite probe. Firstly, 20 mg of the QDs and GO were dissolved separately in 5 mL of Millipore water. Then 5 mL of 0.1 mol L^{-1} EDC was added into the GO solution to activate the carboxylic groups for ~30 min. The QDs solution was then added into the EDC-activated GO solution, followed immediately by the addition of 5 mL of 0.1 mol L^{-1} NHS solution to stabilize the amide linkage formed between the QDs and GO. The reaction was allowed to proceed for 24 hrs and the QD-GO nanocomposite thus formed was purified by the addition of acetone.

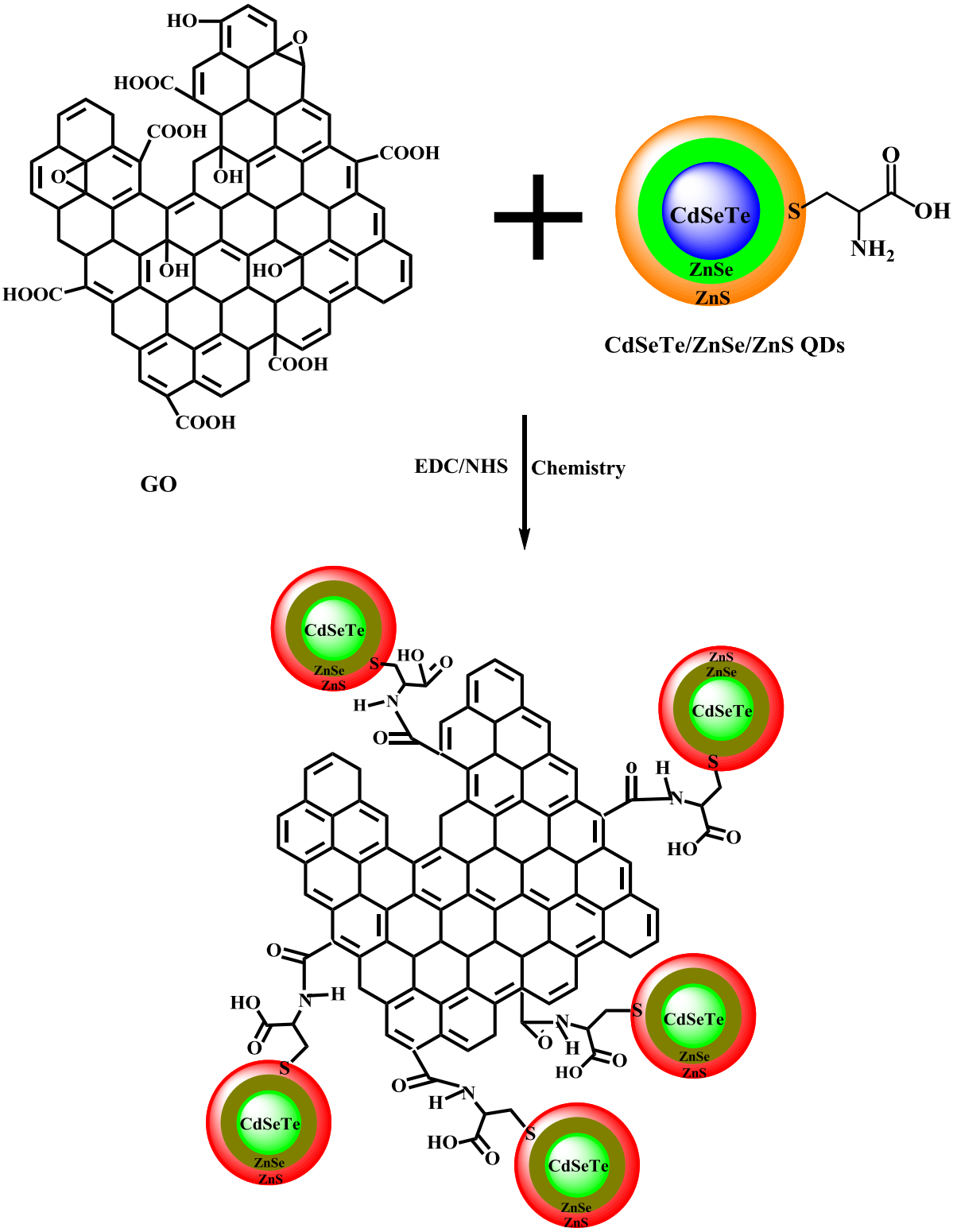

Scheme 1. Schematic representation of the preparation route for the QD-GO nanocomposite probe.

2.7. Procedure for the fluorescent detection of PAHs

The detection of PAHs was carried out in Millipore water. Four PAH analytes (Ant, Naph, Py and Phe) were tested in this work because they are known to be part of the 16 priority PAHs listed by the US Environmental Protection Agency (EPA) **[27]** and have frequently been detected in water systems **[2,5]**. The PAH solutions were prepared in a H_2O/EtOH (2:1) mixture [0 – 5 x 10^{-7} mol L^{-1}]. For fluorescence detection, 0.7 mg/mL of the QD-GO nanocomposite was dissolved in Millipore water and the selected PAH solutions of varying concentration were added at different time intervals. An equilibration time of 5 min was allowed before taking each PL measurement.

3. Results and discussion

3.1. Absorption and PL emission characterization

Fig. 1 shows the absorption and PL emission spectra of the newly synthesized water-soluble L-cysteine-capped CdSeTe/ZnSe/ZnS QDs. A well pronounced and broad excitonic peak at 583 nm and a symmetric PL emission spectrum with a peak at wavelength of 629 nm was obtained for the QDs. The measured PL quantum yield of the QDs was 45% while the estimated full width at half maximum was 60 nm. The PL emission spectrum of the QDs did not show any evidence of deep trap emission mostly inherent in the red tail region, hence suggesting that the QDs exhibited a band edge type of PL emission [28].

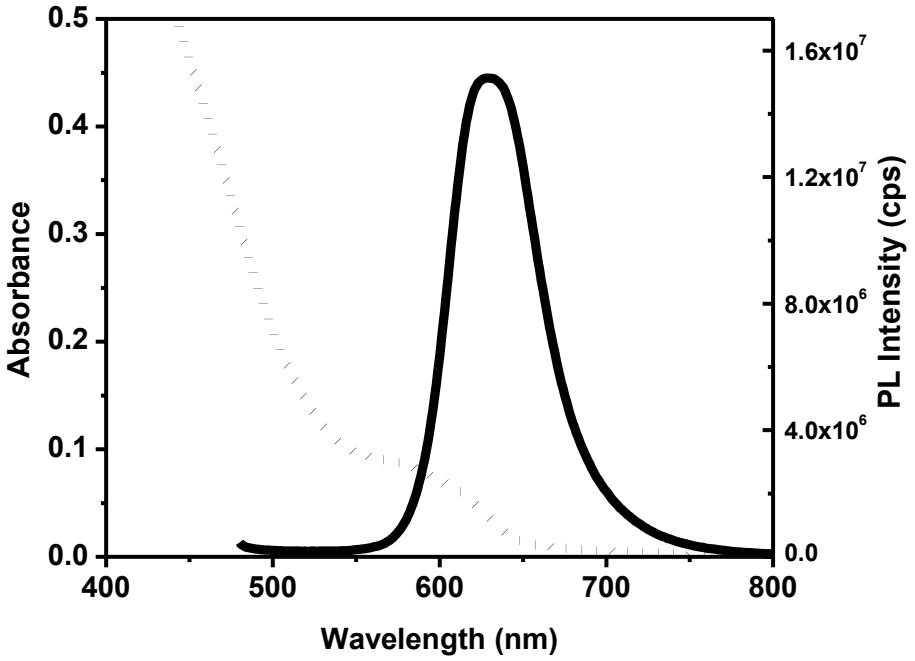

Fig. 1. Absorption (dotted line) and PL emission (solid line) spectra of the water-soluble L-cysteine-capped CdTeSe/ZnSe/ZnS QDs measured in Millipore water at λ_{exc} = 470 nm.

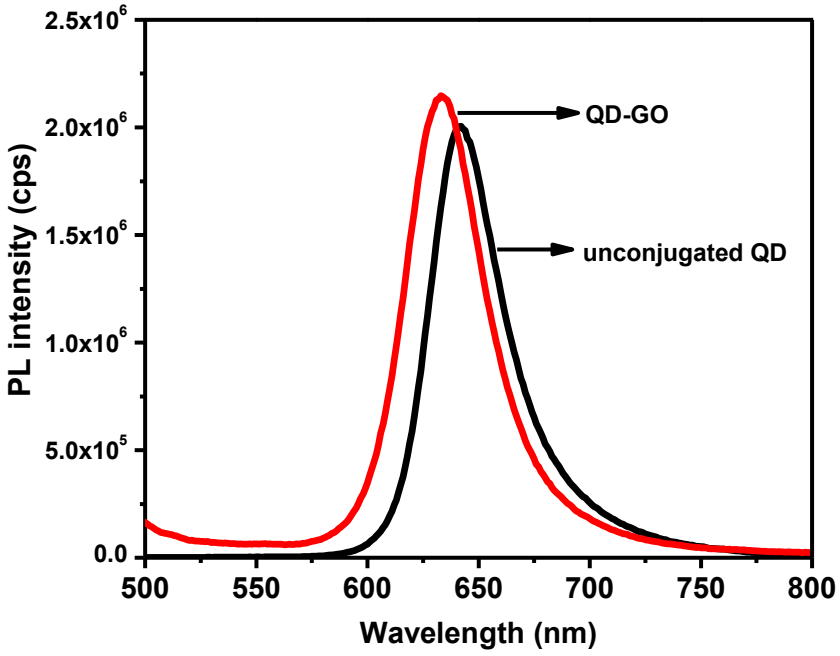

Fig. 2. PL emission spectra of the unconjugated QDs before and after conjugation to GO at λ_{exc} = 470 nm.

Fig. 2 shows the representative PL emission of the unconjugated QDs (measured before conjugation to GO) and the QD-GO nanocomposite. It could be seen that the PL emission of the QD-GO blue-shifted by 9 nm relative to the unconjugated QDs and was also enhanced. The blue-shift in PL emission of the QD-GO indicated that the QDs were not aggregated and that the covalent binding of GO to the QDs increased the band gap. However, the PL emission enhancement effect of the QD-GO nanocomposite observed in this work was in contrast to the PL quenching effect of GO on QDs fluorescence reported by different groups in the literature **[29-31].** Förster resonance energy transfer (FRET) from the QDs (donor) to GO (acceptor) is the sole reported mechanism of interaction between GO and fluorescent emitting QDs. It is important to note that for FRET to occur, quenching of the fluorescence emission of the donor molecule has to be apparent. The lack of quenching of the QD-GO fluorescence found here provided an indication that a different mode of chemical interaction took place between the QDs and GO. We can assume that when phonon energies are equal to or higher than the band gap of the CdSeTe/ZnSe/ZnS nanocrystals, excitation of electrons from the valence band to the conduction band can generate the same amounts of holes in the valence band **[32].** As judged by the QY value of the QDs, the synthesis of the CdSeTe/ZnSe/ZnS QDs may have induced the creation of some surface defect states, thus creating nonradiative exciton dynamics. We believe that upon conjugation of the QDs to GO, conformability between the adsorptive capability of GO and the defect state of the QDs may have induced the PL enhancement effect.

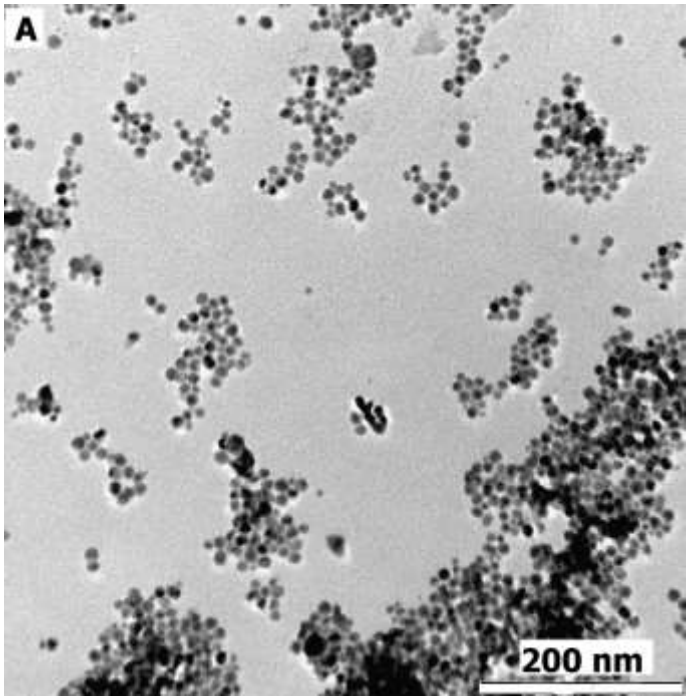
A
200 nm

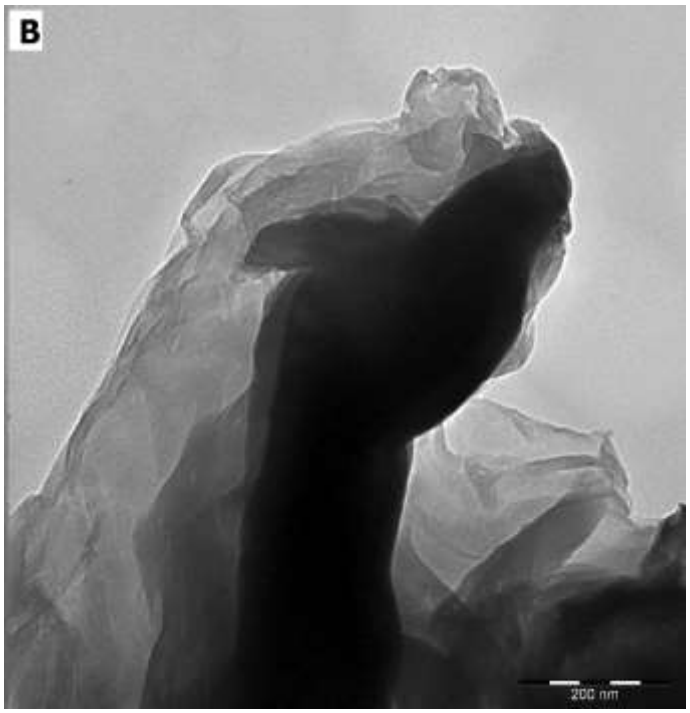
B
200 nm

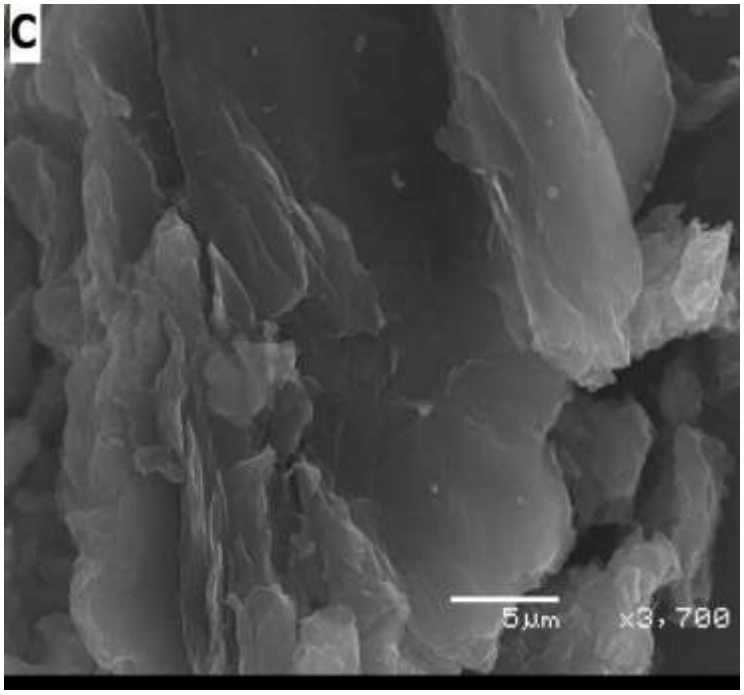
C
5 µm
x3,700

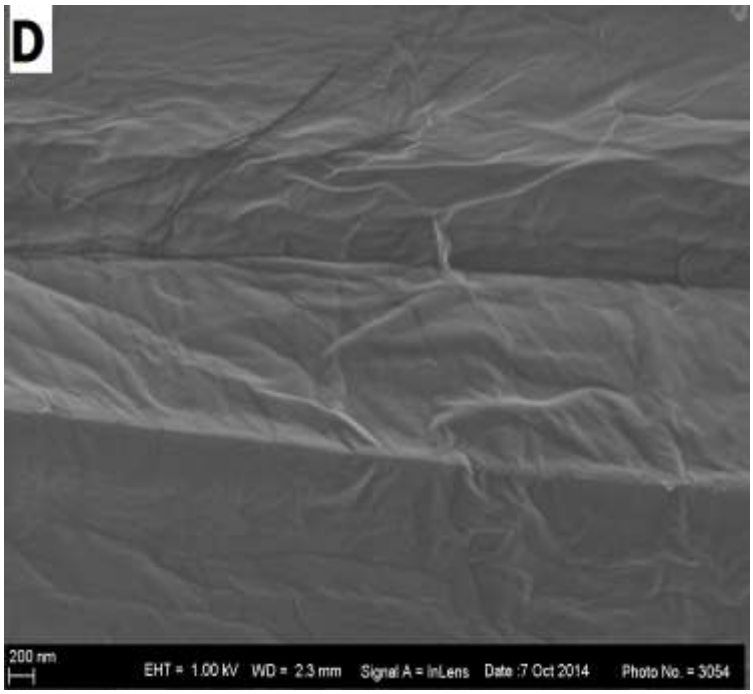
D
200 nm
EHT = 1.00 kV WD = 2.3 mm Signal A = InLens Date :7 Oct 2014 Photo No. = 3054

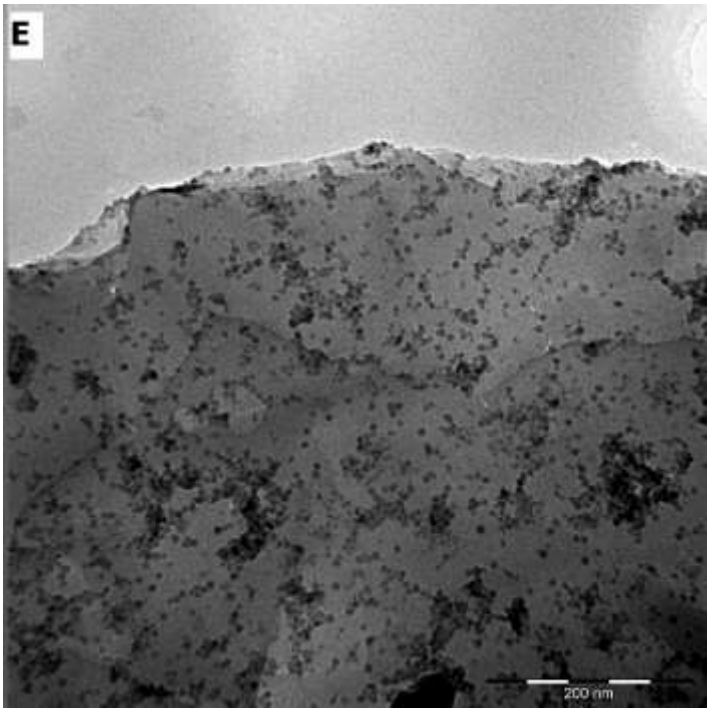

Fig. 3. TEM images of the (A) unconjugated QD and (B) GO. (C) SEM image of GO and (D) HRSEM image of GO (E) TEM image of the QD-GO nanocomposite.

3.2. TEM, SEM and HRSEM analysis

A TEM image of the water-soluble L-cysteine-capped CdSeTe/ZnSe/ZnS QDs is shown in Fig. 3A. It is clearly evident that the QDs were monodispersed and spherical in shape. The morphological display of the QDs also shows that they were nearly homogenous in nature. The estimated average particle size distribution of the QDs was 5.5 nm.

As discussed in Section 2.5, GO was prepared from the exfoliation of graphite oxide. The corresponding TEM image of GO is shown in Fig. 3B. The morphological display of GO did not show any trace of bulk aggregates, but rather the image showed that GO was well exfoliated to individual nanosheets. The SEM image of GO (Fig. 3C) showed a characteristic carbon sheet with crumpled silk waves while the corresponding HRSEM image (Fig. 3D) showed that they were smoothly folded

up into nanosheets. The TEM image of the QD-GO nanocomposite (Fig. 3E) showed that the QDs were effectively anchored onto the graphene sheet with no stand-alone QD nanoparticles lying outside the GO surface, hence confirming the successful conjugation of the QDs to GO.

3.3. XRD analysis

Powder XRD analyses were carried out to investigate the crystal phase nature of the unconjugated QDs, GO and QD-GO nanocomposite, respectively (Fig. 4). The diffraction pattern of GO revealed the presence of the {001} peak at $2\theta = 13.8^{o}$ which was an indication of its characteristic loose-layer-like structure. The interlayer spacing of this peak depends on the water layers in the gallery space of the materials as well as the adopted method of preparation **[33]**. For the unconjugated QDs, the diffraction pattern suggested crystalline nature and corresponds to the typical zinc-blende crystal structure with planes at {111}; $2\theta = 30.7$, {220}; $2\theta = 50.5$ and {311}; $2\theta = 61.1$. In addition, the broad diffraction peaks were a strong indication of the small nanocrystal size of the QDs. Upon conjugation of the QDs to GO, it was evident that the crystallinity of the QDs in the nanocomposite material was retained with no appreciable shift in the peak positions and a weak GO peak in the QD-GO spectrum was observed. This gave a strong indication that the QDs were well immobilized in the GO sheet as confirmed by the TEM image (Fig. 3E).

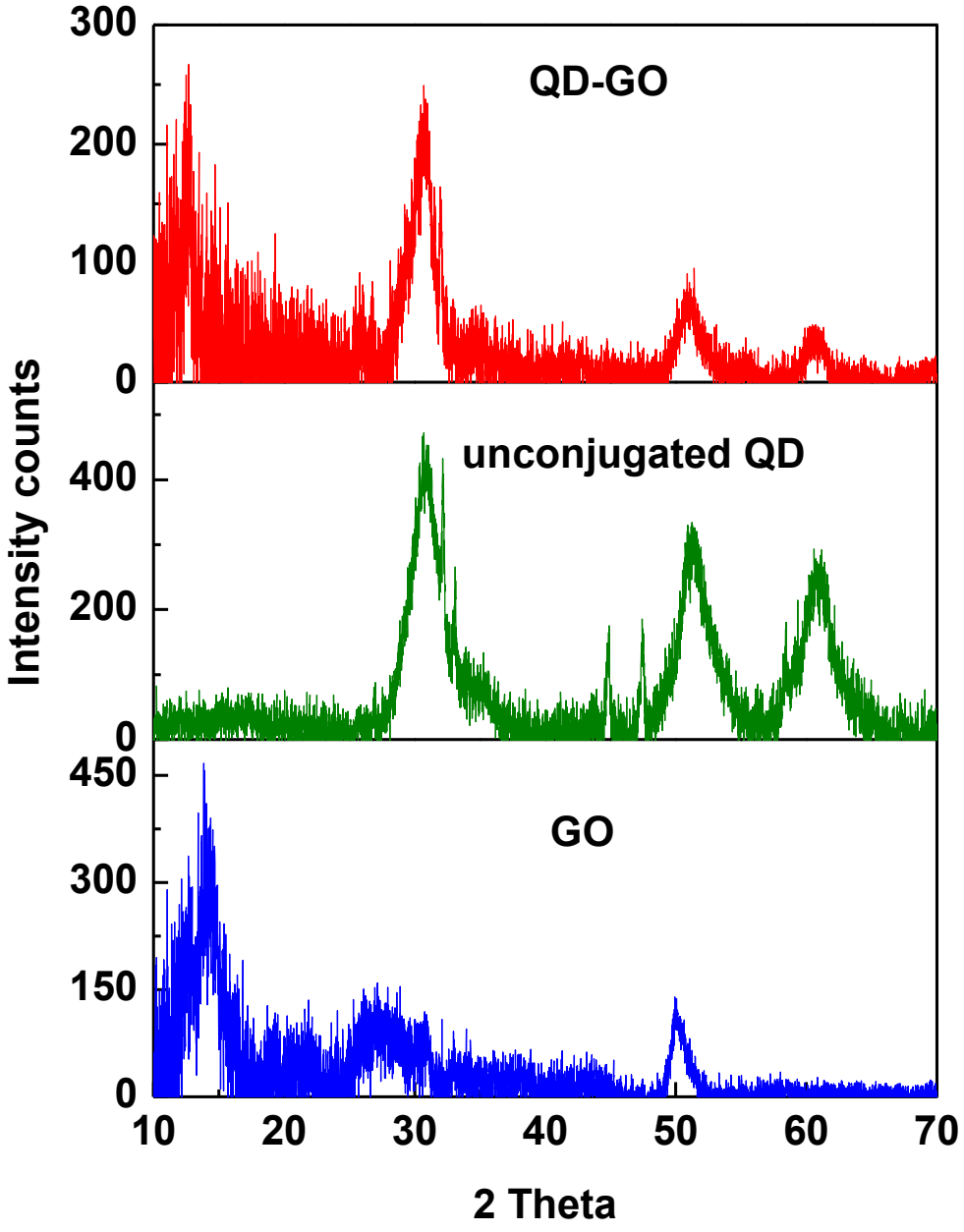

Fig. 4. Powder XRD spectra of GO, unconjugated QD and QD-GO nanocomposite.

3.4. FT-IR analysis

FT-IR analysis was carried out to characterize the functional groups on the surface of the materials. Fig. 5 shows the FT-IR spectra of the GO, unconjugated QDs and QD-GO. For GO, the characteristic bands appeared for carboxylic and carbonyl ($\upsilon_{C=O}$ =

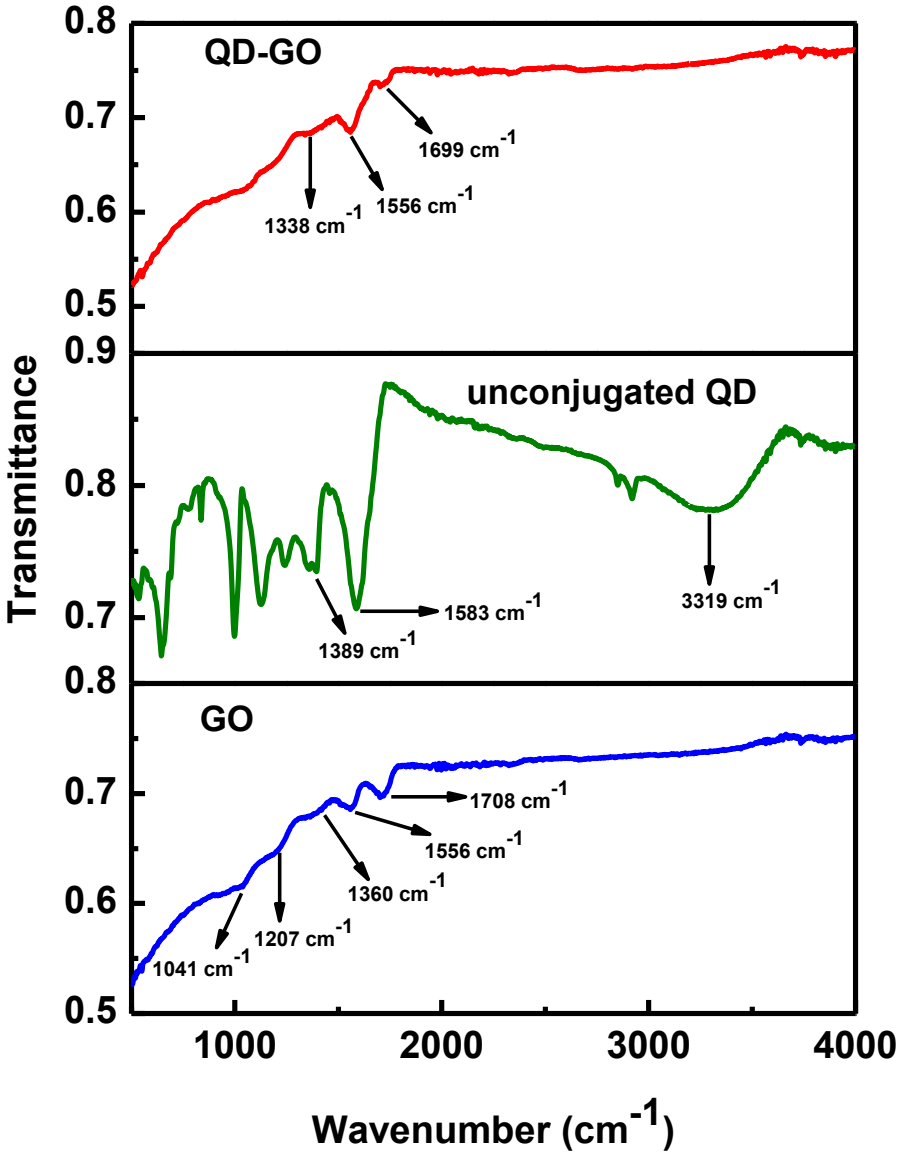

Fig. 5. FT-IR spectra of GO, unconjugated QD and QD-GO nanocomposite.

1708 cm^{-1}), aromatic ($\upsilon_{C=C}$ = 1556 cm^{-1}), carboxy (υ_{C-O} = 1360 cm^{-1}), epoxy (υ_{C-O} = 1207 cm^{-1}) and alkoxy (υ_{C-O} = 1041 cm^{-1}) groups, hence confirming the successful formation of GO. The FT-IR spectrum of the unconjugated QDs revealed the presence of the symmetric and asymmetric carboxylic functional group ($\upsilon_{C=O}$ = 1389 and 1583 cm^{-1}) while the hydroxyl functional group (υ_{O-H} = 3319 cm^{-1}) was also

observed. These were ascribed to the capping agent. In terms of the QD-GO nanocomposite, the FT-IR spectrum was dominated by the GO, however the band appearing at 1699 cm^{-1} could be attributed to the formation of the amide linkage between the QDs and GO.

3.5. RAMAN analysis

The Raman spectra of GO, unconjugated QDs and the QD-GO nanocomposite are shown in Fig. 6. The characteristic D (1350 cm^{-1}) and G (1596 cm^{-1}) bands were recognized on the spectrum of GO **[34]**, hence confirming the successful synthesis of this material. The plane termination of disordered graphite containing vibrating carbon atoms with dangling bonds, corresponds to the D band while the G band was attributed to the vibrating sp^2-bonded carbon atoms **[35]**. The Raman spectrum of the unconjugated QDs displayed a broad and intense optical peak at ~3873 cm^{-1} which was a strong indication of the fluorescence emitting property of the QDs. The Raman spectrum of the QD-GO nanocomposite displayed a similar peak to the unconjugated QDs but had a lower signal intensity. We can attribute the lack of appearance of the GO peaks in the nanocomposite material to be due to the dominance of the fluorescence property of the QD-GO nanocomposite.

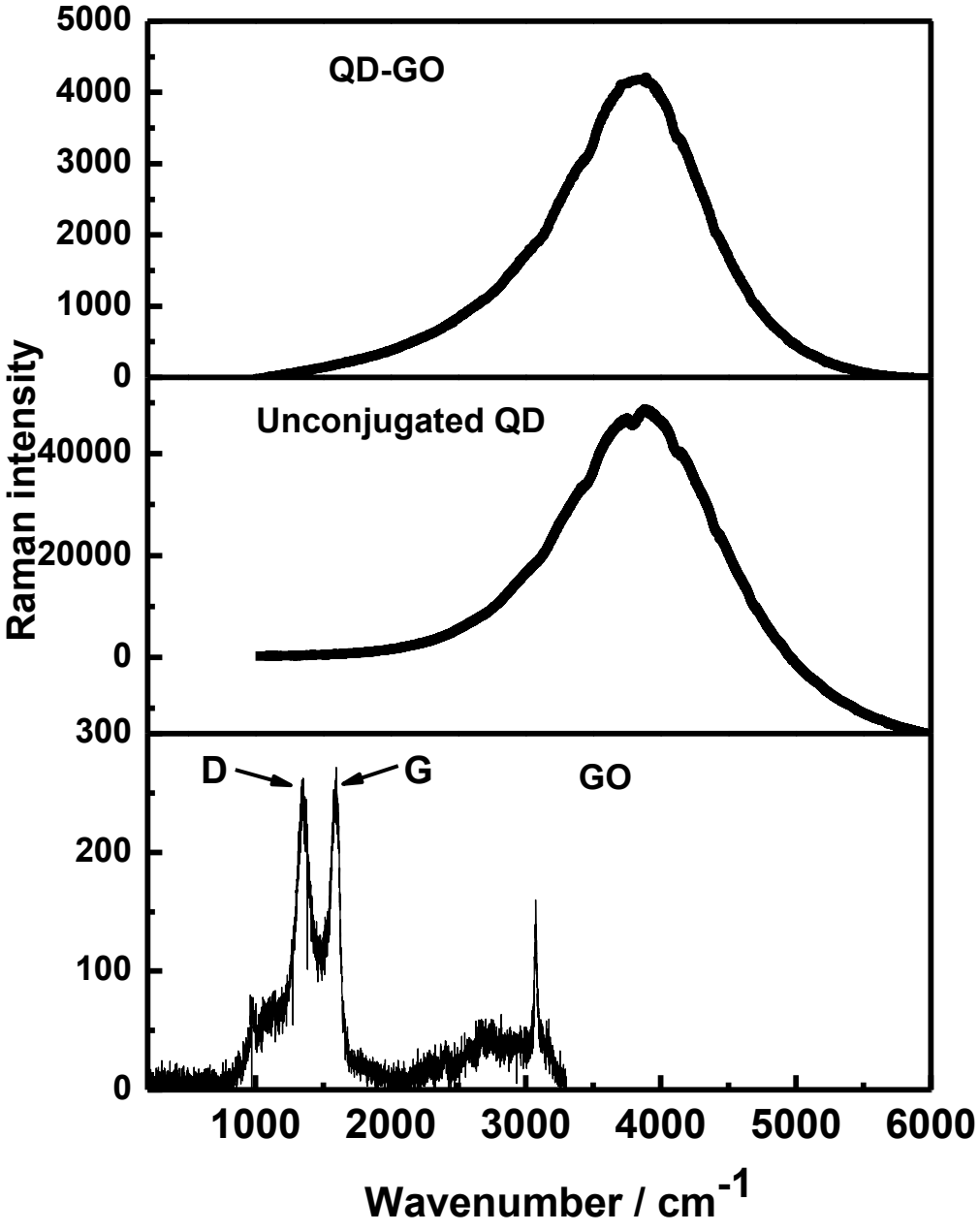

Fig. 6. Raman spectra of GO, unconjugated QDs and QD-GO nanocomposite.

3.6. Application of the QD-GO nanocomposite for PAH PL detection

As discussed in the experimental section, GO was obtained via the chemical exfoliation of graphite oxide. It is important to note that breakage of the extended

two-dimensional stacked π-conjugation of the graphene nanosheets was due to the oxidation of graphite which thus resulted in hybridized sp^2 nanoscale graphitic domains which were surrounded by defect carbon vacancies as well as oxidized and highly disordered sp^3 domains. The resultant GO nanosheets were characterized by hydroxyl and derivatized carboxylic groups at the edges, with phenolic and epoxy groups lying predominantly at the basal plane **[36,37]**. Based on this chemical functionality of GO, the nanosheets were readily exfoliated to form a light brown coloured, stable and dispersible suspension in water, which was required for the use of the QD-GO nanocomposite as a material for the sensing of environmental contaminants in water, as in this study.

In this work, the advantage of using GO was not only limited to its large surface area, but was also based on the nature of the chemical structure of GO. The strong π-π interaction induced by the hexagonal array of carbon atoms in the GO nanosheet provides a unique platform to adsorb analytes with fused benzene rings. Fig. 7 shows the PL analytical response of the fluorescence of the QD-GO nanocomposite probe obtained when a fixed concentration of 5×10^{-7} mol L^{-1} of Naph, Ant, Py and Phe were tested, respectively. We employed an equilibration time of 5 min before taking each of the fluorescence measurements. PAHs have fused benzene rings, hence enhancing their affinity for the QD-GO probe. From Fig. 7, it is clear that each of these ubiquitous PAH analytes can be detected using the QD-GO probe with the PL enhancement effect following the order: Phe > Ant > Py ≥ Naph, therefore we chose to select Phe for further PL testing using the QD-GO nanocomposite probe.

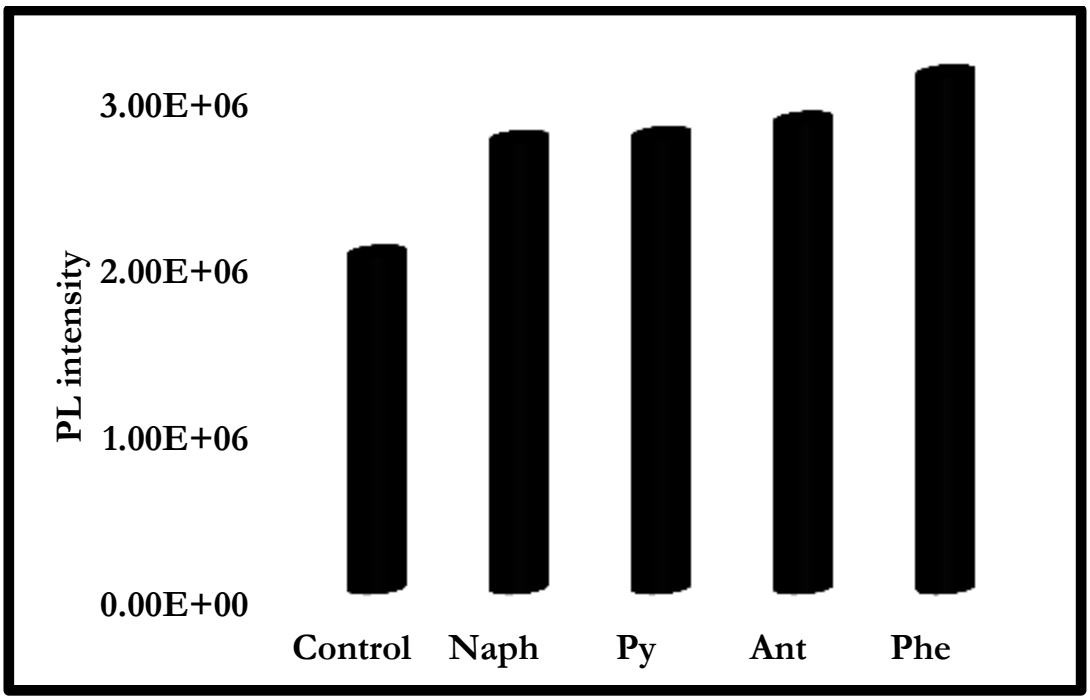

Fig. 7. Effect of a fixed concentration of 5 x 10^{-7} mol L^{-1} of Naph, Ant, Py and Phe on the fluorescence intensity of the QD-GO nanocomposite probe at 633 nm. Control = QD-GO (0.7 mg/mL).

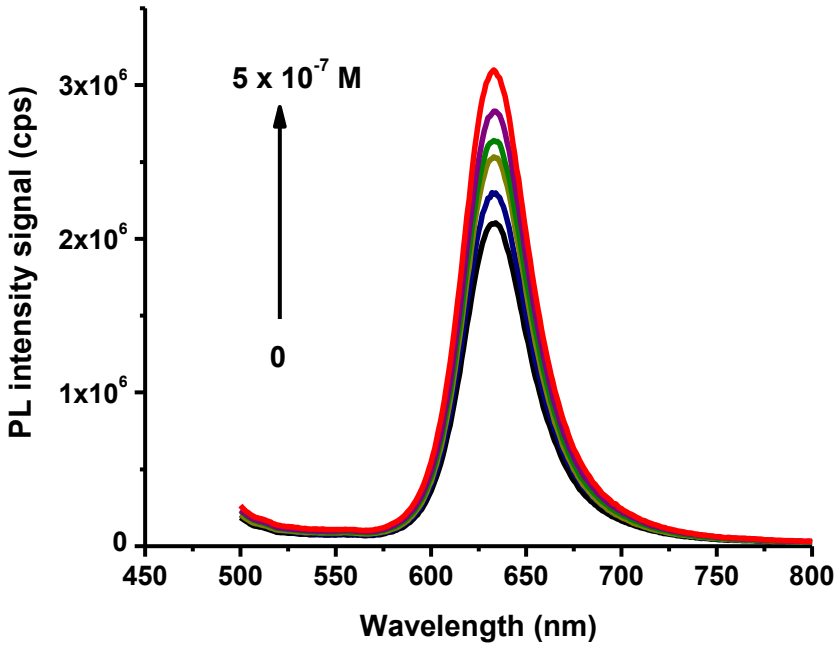

Fig. 8. Fluorescence detection of phenanthrene at increasing concentration corresponding to a steady enhancement in PL signal of the QD-GO nanocomposite probe. [Phe] = 0, 1 x 10^{-7}, 2 x 10^{-7}, 3 x 10^{-7}, 4 x 10^{-7} and 5 x 10^{-7} mol L^{-1} (λ_{exc} = 470 nm).

Under optimum conditions in terms of the absence of matrix or interfering analytes, the detection of Phe using the QD-GO nanocomposite probe was carried out at varying concentrations of the analyte. As shown in Fig. 8, the PL intensity of the QD-GO probe at 633 nm was progressively enhanced as the concentration of Phe was increased. The detection of Phe did not induce any noticeable shift in the PL emission of the probe. We attributed this to the high stability of the probe. The linear regression curve for the detection of Phe is shown in Fig. 9, with the concentration of

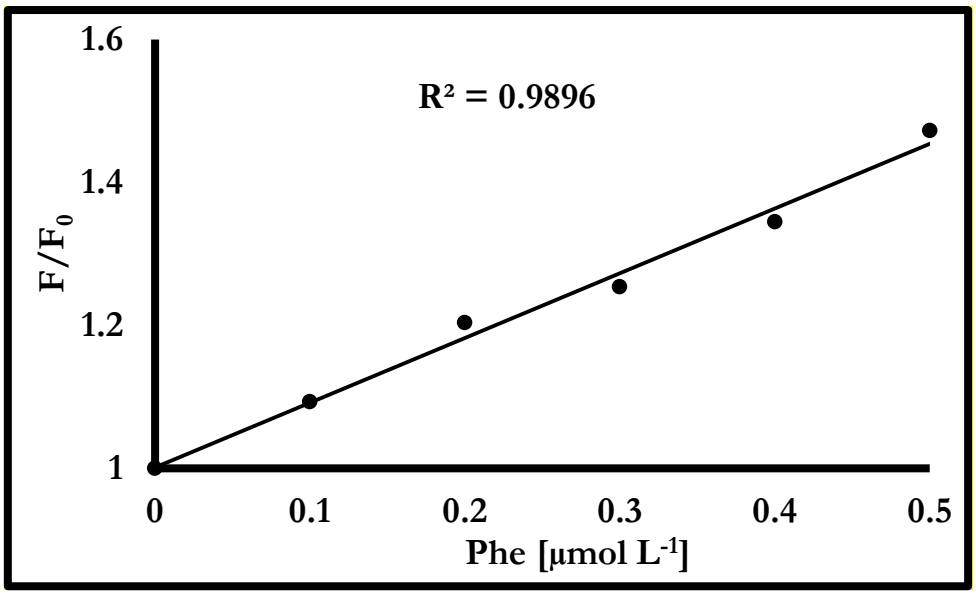

Fig. 9. Calibration regression curve showing the linear response of the QD-GO nanocomposite probe upon detection of phenanthrene. F_0 is the fluorescence intensity of the QD-GO nanocomposite without the analyte and F is the fluorescence intensity after addition of the analyte.

the analyte in the range of 0 - 5 x 10^{-7} mol L^{-1}. The limit of detection (LOD) was calculated using the equation $3\delta/K$, where K is the slope of the calibration graph and δ is the standard deviation of blank measurements (n =10). The LOD obtained for Phe was thus 1.07 x 10^{-9} mol L^{-1} or 0.19 µg/L which indicated that this method holds promise for use in environmental monitoring, as the maximum allowable

concentration for Phe in water is 3.0 mg/L **[38],** whilst reported concentrations of Phe in river water in South Africa ranges from 0.053 – 0.616 µg/L **[2]**.

The PL enhancement effect of the four tested PAHs differed slightly from each other. From the relative PL enhancement at 633 nm, the LODs of Ant, Naph and Py were estimated to be ~0.26 µg/L. It is important to note that each of the PAH compounds differ mainly in their aromaticity, number of fused benzene rings and molecular shape. We believe that the trend in the PL enhancement effect of the PAHs samples was synonymous to their adsorption affinity for the QDs-GO probe. Because PAHs are known to act as π-electron donors due to their high electron density, the overall reaction mechanism (Scheme 2) can be explained based on the interaction between the electron-rich π-system of the PAH molecule and the π-electron system of the graphene material, which thus leads to an adsorption-PL enhancement effect exhibited by QD-GO probe, making it suitable for the detection of this class of compounds.

4. Conclusions

In summary, alloyed L-cysteine-capped CdSeTe/ZnSe/ZnS core/shell/shell QDs were synthesized for the first time and covalently bonded to GO, hence forming a novel QD-GO nanocomposite probe. Comparison of the PL spectra of the unconjugated QD and the QD-GO nanocomposite showed that the later was enhanced relative to the former. Four ubiquitous priority PAH analytes, namely Naph, Ant, Py and Phe were tested for their affinity to adsorb onto the modified GO

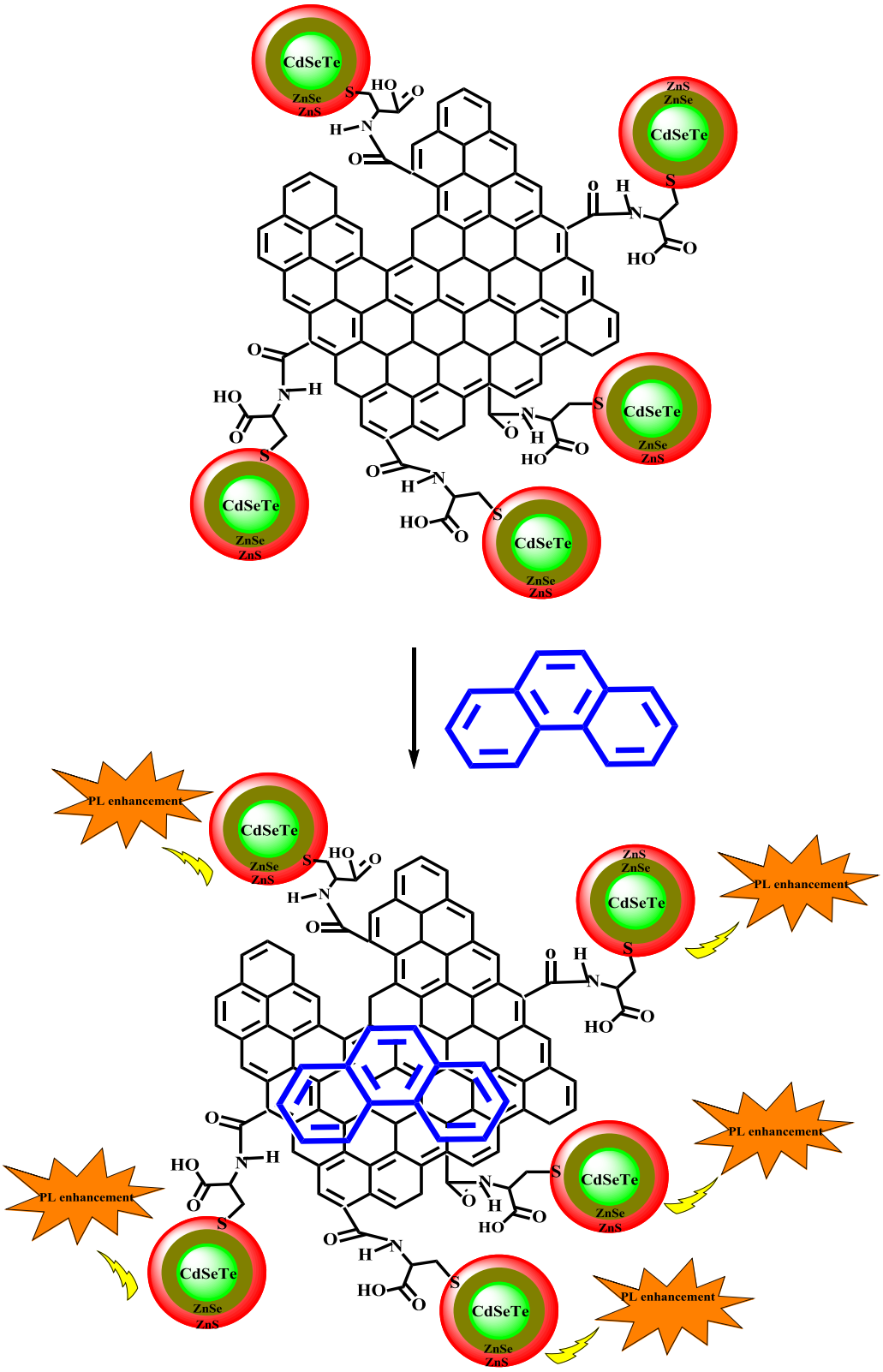

Scheme 2. Proposed fluorescence detection mechanism of phenanthrene using the QD-GO nanocomposite probe.

and thus influence the PL intensity of the conjugated QDs. Results showed that the PL enhancement effect was greatest for Phe therefore it was selected for further PL studies. Detection of Phe was successfully carried out in aqueous media with a LOD of 0.19 μg/L, whilst the LOD of Ant, Naph and Py were estimated to be ~0.26 μg/L. The simplicity, low cost and low LOD of the sensor demonstrates its potential for application as a screening tool for PAH compounds in environmental water pollution monitoring. Additional selectivity studies are required in order to determine the effect of potentially interfering compounds in real environmental samples on PAH detection.

Acknowledgements

A postdoctoral fellowship offered by the University of Pretoria is gratefully appreciated by O. Adegoke. This work is based on research supported in part by the National Research Foundation of South Africa, Grant Numbers: 90720 and 93394 (P. Forbes), as well as the Department of Science and Technology (DST) through the Photonics Initiative of South Africa (grant PISA-15-DIR-06), and the Water Research Commission (grant K5-2438). Wirsam Scientific, South Africa is thanked for their support of this research. We thank the Electron Microscopy Unit, University of Pretoria (UP), for assistance with the TEM measurements and Wiebke Grote of UP for the XRD measurements.

References

1. M J. Jacob, W. Karcher, R. Dumler, J.J. Belliardo, A. Boenke, Polycyclic aromatic compounds of environmental and occupational importance-Their occurrence, toxicity and the development of high-purity certified reference materials Part III. J. Anal. Chem. 340 (1991) 755-767.
2. L. Chimuka, P. Sibiya, R. Amdany, E. Cukrowska, P.B.C. Forbes, Status of PAHs in environmental compartments of South Africa: A country report. Polycycl. Aromat. Comp. (2015) DOI: 10.1080/10406638.2014.988276.
3. Y. Kameda, J. Shirai, T. Komai, J. Nakanishi, S. Masunaga, Atmospheric polycyclic aromatic hydrocarbons: size distribution, estimation of their risk and their depositions to the human respiratory tract. Sci. Total Environ. 340 (2005) 71-80.
4. N. Vardar, Y. Tasdemir, M. Odabasi, K.E. Noll, Characterization of atmospheric concentrations and partitioning of PAHs in the Chicago atmosphere. Sci. Total Environ. 327 (2004) 163- 174.
5. E. Martinez, M. Gros, S. Lacorte, D. Barceló, Simplified procedures for the analysis of polycyclic aromatic hydrocarbons in water, sediments and mussels. J. Chrom. A 1047 (2004) 181-188.
6. P.B.C. Forbes, E.R. Rohwer, Monitoring of trace organic air pollutants – a developing country perspective, Air Pollution XVI, WIT Transactions on Ecology and the Environment. 116 (2008) 345-355, ISSN 1743-3541.

7. X. Wang, B. Liu, Q. Lu, Q. Qu, Graphene-based materials: fabrication and application for adsorption in analytical chemistry. J. Chromatogr. A 1362 (2014) 1-15.
8. R. Shi, L. Yan, T. Xu, D. Liu, Y. Zhu, J. Zhou, Graphene oxide bound silica for solid-phase extraction of 14 polycyclic aromatic hydrocarbons in mainstream cigarette smoke. J. Chromatogr. A 1375 (2015) 1-7.
9. F. Wang, J.J.-H Haftka, T.L. Sinnige, J.L.M. Hermens, W. Chen, Adsorption of polar, nonpolar, and substituted aromatics to colloidal graphene oxide nanoparticles. Environ. Pollut. 186 (2014) 226-233.
10. S. Chowdhury, R. Balasubramanian, Recent advances in the use of graphene-family nanoadsorbents for removal of toxic pollutants from wastewater. Adv. Colloid Interfac. 204 (2014) 35–56.
11. S. Basu, P. Bhattacharyya, Recent developments on graphene and graphene oxide based solid state gas sensors. Sensor. Actuat. B-Chem. 173 (2012) 1– 21.
12. M. Valcarcel, S. Cárdenas, B. Simonet, Y. Moliner-Martinez, R. Lucena, Carbon nanostructures as sorbent materials in analytical processes. Trends Anal. Chem. 27 (2008) 34–43.
13. J-S. Cheng, J. Du, W. Zhu, Facile synthesis of three-dimensional chitosan–graphene mesostructures for reactive black 5 removal. Carbohydr. Polym. 88 (2012) 61-67.
14. Y. Xu, L. Zhao, H. Bai, W. Hong, C. Li, G. Shi, Chemically converted graphene induced molecular flattening of 5, 10, 15, 20-tetrakis (1-methyl-4-pyridinio)

porphyrin and its application for optical detection of cadmium (II) ions. J. Am. Chem. Soc. 131 (2009) 13490-13497.

15. A. Gutes, B. Hsia, A. Sussman, W. Mickelson, A. Zettl, C. Carraro, R. Maboudian, Graphene decoration with metal nanoparticles: towards easy integration for sensing applications. Nanoscale 4 (2012) 438-440.
16. A.A. Farghali, M. Bahgat, W.M.A. El Rouby, M.H. Khedr, Preparation, decoration and characterization of graphene sheets for methyl green adsorption. J. Alloys Compd. 555 (2013) 193-200.
17. S.J. Rosenthal, J. McBride, S.J. Pennycook, L.C. Feldman, Synthesis, surface studies, composition and structural characterization of CdSe, core/shell, and biologically active nanocrystals. Surf. Sci. Rep. 62 (2007) 111–157.
18. R. Gill, M. Zayats, I. Willner, Semiconductor quantum dots for bioanalysis. Angew. Chem. Int. Ed. 47 (2008) 7602-7625.
19. G. Zhiguo, Y. Shuping, L. Zaijun, S. Xiulan, W. Guangli, F. Yinjun, L. Junkang, Multiple headspace solid-phase microextraction after matrix modification for avoiding matrix effect in the determination of ethyl carbamate in bread. Anal. Chim. Acta 701 (2011) 75-80.
20. M. Alibolandi, F. Hadizadeh, F. Vajhedin, K. Abnous, M. Ramezani, Design and fabrication of an aptasensor for chloramphenicol based on energy transfer of CdTe quantum dots to graphene oxide sheet. Mat. Sci. Eng. C-Mater. 48 (2015) 611–619.

21. M. Li, X. Zhou, S. Guo, N. Wu, Detection of lead (II) with a "turn-on" fluorescent biosensor based on energy transfer from CdSe/ZnS quantum dots to graphene oxide. Biosens. Bioelectron. 43 (2013) 69–74.
22. G. Zhiguo, Y. Shuping, L. Zaijun, S. Xiulan, W. Guangli, F. Yinjun, L. Junkang, An ultrasensitive electrochemical biosensor for glucose using CdTe-CdS core-shell quantum dot as ultrafast electron transfer relay between graphene-gold nanocomposite and gold nanoparticle. Electrochim. Acta 56 (2011) 9162– 9167.
23. D. Magde, R. Wong, P.G. Seybold, Fluorescence quantum yields and their relation to lifetimes of rhodamine 6G and fluorescein in nine solvents: improved absolute standards for quantum yields. Photochem. Photobiol. 75 (2002) 327-334.
24. B.C. Fitzmorris, Y-C. Pu, J.K. Cooper, Y-F. Lin, Y-J. Hsu, Y. Li, J.Z. Zhang, Optical properties and exciton dynamics of alloyed core/Shell/Shell Cd1–x Zn x Se/ZnSe/ZnS quantum dots. Appl. Mater. Interfaces 5 (2013) 2893-2900.
25. W. Zhang, G. Chen, J. Wang, B-C. Ye, X. Zhong, Design and synthesis of highly luminescent near-infrared-emitting water-soluble CdTe/CdSe/ZnS core/shell/shell quantum dots. Inorg. Chem. 48 (2009) 9723-9731.
26. W.S. Hummers Jr., R.E. Offeman, Preparation of graphitic oxide. J. Am. Chem. Soc. 80 (1958) 1339.
27. US Environmental Protection Agency, Guidelines establishing test procedures for the analysis of pollutants, Proposed regulations, Federal Register, vol. 49, no. 209, USEPA, Washington, DC.
28. B. De Geyter, Y. Justo, I. Moreels, K. Lambert, P. F. Smet, D. Van Thourhout, A.J. Houtepen , D. Grodzinska, C. de Mello Donega, A. Meijerink, D.

Vanmaekelbergh, Z. Hens, The different nature of band edge absorption and emission in colloidal PbSe/CdSe core/shell quantum dots. ACS Nano 5 (2011) 58-66.

29. M. Liu, H. Zhao, X. Quan, S. Chen, X. Fan, Distance-independent quenching of quantum dots by nanoscale-graphene in self-assembled sandwich immunoassay. Chem. Commun. 42 (2010) 7909–7911.
30. Z. Chen, S. Berciaud, C. Nuckolls, T.F. Heinz, L.E. Brus, Energy transfer from individual semiconductor nanocrystals to graphene. ACS Nano 5 (2010) 2964–2968.
31. E. Marales-Narváez, B. Pérez-López, L.B. Pires, A. Merkoçi, Simple Förster resonance energy transfer evidence for the ultrahigh quantum dot quenching efficiency by graphene oxide compared to other carbon structures. Carbon 50 (2012) 2987-2993.
32. Q. Wang, B. Geng, S. Wang, ZnO/Au hybrid nanoarchitectures: wet-chemical synthesis and structurally enhanced photocatalytic performance. Environ. Sci. Technol. 43 (2009) 8968–8973.
33. Z.H. Liu, Z.M. Wang, X.J. Yang, K. Ooi, Intercalation of organic ammonium ions into layered graphite oxide. Langmuir 18 (2002) 4926–4932.
34. D. Yang, A. Velamakanni, G. Bozoklu, S. Park, M. Stoller, R.D. Piner, S. Stankovich, I. Jung, D.A. Field, C.A. Ventrice, R.S. Ruoff, Chemical analysis of graphene oxide films after heat and chemical treatments by X-ray photoelectron and Micro-Raman spectroscopy. Carbon 47 (2009) 145-152.

35. W. Wei, D.M. Zhang, L.H. Yin, Y.P. Pu, S.Q. Liu, Colorimetric detection of DNA damage by using hemin-graphene nanocomposites. Spectrochim. Acta A 106 (2013) 163–169.
36. A. Lerf, H. He, M. Forster, J. Klinowski, Structure of graphite oxide revisited. J. Phys. Chem. B 102 (1998) 4477-4482.
37. W. Gao, L.B. Alemany, L. Ci, P.M. Ajayan, New insights into the structure and reduction of graphite oxide. Nat. Chem. 1 (2009) 403-408.
38. Agency for Toxic Substances and Disease Registry (ATSDR). 2006. Toxicological Profiles CD-ROM. ATSDR: Washington, USA.